BIOCHEMISTRY
including biophysical chemistry & molecular biology

Article

pubs.acs.org/biochemistry

Critical Evaluation of the Two-State Model Describing the Equilibrium Unfolding of the PI3K SH3 Domain by Time-Resolved Fluorescence Resonance Energy Transfer

Megha Kishore,[†] G. Krishnamoorthy,*[,‡] and Jayant B. Udgaonkar*[,†]

[†]National Centre for Biological Sciences, Tata Institute of Fundamental Research, Bangalore 560065, India

[‡]Department of Chemical Sciences, Tata Institute of Fundamental Research, Mumbai 400005, India

Supporting Information

ABSTRACT: It appears that equilibrium unfolding transitions of many small proteins can be described as two-state transitions, because the probes commonly used to measure such transitions cannot detect the underlying heterogeneity inherent in protein folding and unfolding reactions. Time-resolved fluorescence or Forster resonance energy transfer (TRFRET) measurements have the potential to uncover such heterogeneity and to test the cooperativity of protein folding reactions. Here, TRFRET measurements have been used to study the equilibrium unfolding of the SH3 domain of PI3 kinase. The single tryptophan residue (W53) was used as the FRET donor, and a covalently attached thionitrobenzoate moiety at either of two sites (C17 and C70) was used as the FRET acceptor. The individual lifetime and amplitude components estimated from fitting the fluorescence decay kinetics to the sum of three or four exponentials were determined over a range of denaturant concentrations. The equilibrium unfolding transitions reported by these components were found to be noncoincident, suggesting the presence of multiple conformations in equilibrium during the course of unfolding. Fluorescence lifetime distributions were also generated by the model-free maximum entropy method of analysis. Different segments of the protein were found to show differences in the expansion of the native state at low denaturant concentrations, suggestive of gradual structural transitions. The unfolded protein was found to swell at increasingly high denaturant concentrations. The evolution of the fluorescence lifetime distributions with increasing denaturant concentration was also found to be incompatible with a two-state equilibrium unfolding model.

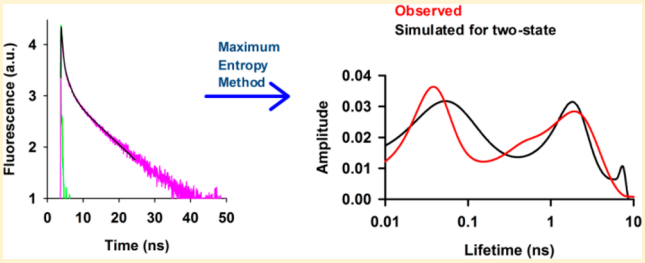

SH3 domains have been studied widely as models for "two-state" protein folding. These small domains are found as parts of many large, multidomain proteins involved in signal transduction, where they serve as scaffolds for the recruitment of other proteins.[1] The SH3 domain of PI3 kinase (the PI3K SH3 domain) is one such model system whose folding mechanism has been studied in detail.[2−6] Although the earliest studies of the folding of the PI3K SH3 domain[7] suggested that this protein was a classic two-state folder, later studies utilizing multiple steady-state probes allowed the identification and characterization of intermediates on the folding pathway.[2,3]

Both equilibrium and kinetic studies have shown that intermediates are populated during the folding and unfolding of the PI3K SH3 domain.[2] Folding has been shown to commence with a submillisecond, nonspecific chain collapse reaction, which appears to be gradual in nature.[4] Under strongly stabilizing conditions, the submillisecond folding reactions are not just of nonspecific chain collapse but culminate in the formation of a specific structured intermediate.[3] A study of unfolding utilizing native-state hydrogen exchange assayed by mass spectrometry (HX-MS) also suggested that unfolding and folding in the absence of a denaturant, as well as in the presence of a very low denaturant concentration, occur through an intermediate and implicated gradual structural transitions in both processes.[5] An intermediate populated at a high denaturant concentration has been shown to possess non-native structure.[6] Although there is convincing evidence that the PI3K SH3 domain does not fold in a two-state manner, a good measure of conformational heterogeneity at various stages of folding of this protein is still lacking.

One way to measure conformational heterogeneity during the course of a protein folding or unfolding reaction is to use time-resolved fluorescence or Forster resonance energy transfer (TRFRET) measurements. The distribution of fluorescence lifetimes of a donor fluorophore in the presence of a FRET acceptor is measured and translated into a distribution of intramolecular distances between the donor and acceptor. TRFRET measurements have not only revealed incremental, noncooperative unfolding in the case of barstar and monellin but also revealed the evolution of conformational hetero-

Received: September 27, 2013
Revised: December 4, 2013
Published: December 10, 2013

   dx.doi.org/10.1021/bi401337k | *Biochemistry* 2013, 52, 9482−9496

geneity.[8−10] They have been used to demonstrate the asynchronous unfolding of different segments of *Escherichia coli* adenylate kinase[11−13] and to characterize collapsed states of cytochrome *c*.[14−16] These studies have firmly established TRFRET as a powerful experimental probe for studying structural and dynamic aspects of protein folding reactions and investigating conformational heterogeneity during folding−unfolding transitions.

An intrinsic tryptophan residue is usually used as the donor fluorophore in TRFRET studies. The main complication in studying time-resolved tryptophan fluorescence is that the fluorescence decay is described normally, with few exceptions,[8,17,18] not as a single-exponential process but as a multiexponential process.[19−22] The origin of multiple fluorescence lifetimes exhibited by a single tryptophan residue in a protein is poorly understood[20,21,23] and is ascribed usually to multiple static protein conformations, each with a discrete tryptophan fluorescence lifetime.[21,24−26] Such a physical model does not, however, appear to be satisfactory for protein molecules that are known to undergo internal dynamic motion over a wide time scale, from picoseconds to hundreds of seconds.[27−30] Hence, a continuous distribution of fluorescence lifetimes seems to be a more appropriate description of the fluorescence decay of a tryptophan residue in a protein, and several procedures for modeling fluorescence lifetime distributions in proteins have emerged. Some procedures use Gaussian or Lorentzian models to represent distributions of fluorescence lifetimes,[31−33] but the primary assumption about the shape of the distributions may not be realistic. On the other hand, the maximum entropy method (MEM) for the analysis of fluorescence intensity decays[34−36] is a model-free approach that relies only on information contained within the experimental decay and makes no assumptions about the resultant distribution profiles. The lifetime distribution profile can then be interpreted in terms of the ensemble properties of the different forms of the protein present. MEM analysis of time-resolved fluorescence data has been successfully applied to study protein folding and dynamics in several model systems.[8,14−16,37]

In this study, the extent of conformational heterogeneity during the unfolding of the PI3K SH3 domain has been explored by using TRFRET to follow the equilibrium unfolding transitions induced by two different denaturants. Intramolecular distances separating the single tryptophan residue (W53) in the protein from either residue C17 in an N-terminal loop region or C70 in the C-terminal short loop (Figure 1) have been monitored. The noncoincident unfolding transitions upon which the individual lifetime and amplitude components obtained by discrete analysis report indicate significant structural heterogeneity in the equilibrium transitions. The evolution of fluorescence lifetime distributions, obtained by MEM analysis, has been analyzed quantitatively. Evidence of the gradual expansion of the native state at low denaturant concentrations and site-specific differences in global fits to a two-state equilibrium unfolding model also indicate that the unfolding of the PI3K SH3 domain cannot be described by models that invoke only a few discrete states.

MATERIALS AND METHODS

Protein Expression, Purification, and Labeling. The gene encoding the PI3K SH3 domain with the first serine residue deleted was cloned into the pET 22b+ vector. Two single-cysteine mutations were generated in this background using the QuikChange kit.[4] Both mutant proteins, Cys17 and Cys70, were expressed in *E. coli* BL21 DE(*)3 competent cells and purified using a protocol described previously.[2] The purity of each protein was confirmed by electrospray ionization mass spectrometry (ESI-MS), using a SYNAPT G2 mass spectrometer.

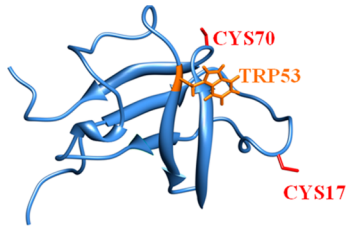

Figure 1. Structure of the PI3K SH3 domain. The highlighted residues have been used for FRET measurements. W53 is located at the beginning of the third β strand. C17 is located in the middle of a long loop region (RT loop) in the N-terminus, which is functionally important for binding substrate proteins.[64] C70 is located in the short tripeptide loop connecting the last two β-strands. The estimated C_α−C_α distances are 14.9 and 9.1 Å for the W53−C17 and W53−C70 FRET pairs, respectively. The image of the structure (Protein Data Bank entry 1pnj) was created using Chimera (University of California, San Francisco).[65]

The single cysteine residue in the protein was covalently conjugated to a TNB moiety that serves as an acceptor for tryptophan fluorescence. The labeling protocol was identical to that described previously.[4] The mass of each labeled protein showed the expected increase of 196 Da, corresponding to the mass of the TNB group, and all proteins were >95% labeled as confirmed by ESI-MS.

Buffers and Reagents. All buffers and chemical reagents used were of the highest purity available from Sigma. Ultrapure grade guanidine hydrochloride (GdnHCl) and urea were obtained from USB Corp. All experiments were conducted in 20 mM sodium phosphate (pH 7.2) at 25 °C. All buffers were routinely filtered through a 0.22 μm filter before being used. Cys17 and Cys70 mutant proteins treated with and without 1 mM DTT showed no difference in fluorescence spectra, implying that no intermolecular disulfide-bonded dimers formed during the experiment.[38] All subsequent experiments were conducted under identical conditions, without DTT, for both the unlabeled and labeled proteins. Concentrations of stock solutions of urea and GdnHCl were determined by measuring refractive indices on an Abbe refractometer. Concentrations of protein stock solutions were determined and corrected for the TNB contribution as described previously.[4] For all equilibrium unfolding transitions, the protein was incubated in buffer for ≥4 h before the experiments.[2]

Spectroscopic Measurement of Conformational Stability. To measure the conformational stabilities of the proteins, equilibrium unfolding transitions were monitored on the MOS-450 instrument (Bio-Logic Inc.) using tyrosine fluorescence as a probe. The native protein was incubated in increasing concentrations of denaturant (GdnHCl from 0 to 6 M or urea from 0 to 9 M). The tyrosine residues were selectively excited at 268 nm, and fluorescence emission was recorded through a 300 nm bandpass filter.

Time-Resolved Fluorescence Measurements. Fluorescence intensity decays were measured at increasing concentrations of denaturant (GdnHCl from 0 to 6 M and urea from 0

dx.doi.org/10.1021/bi401337k | *Biochemistry* 2013, 52, 9482−9496

to 9 M) for the unlabeled and labeled proteins. For this purpose, 885 nm radiation from a femtosecond/picosecond Ti-sapphire laser (Tsunami, Spectra Physics), pumped by an Nd:YVO_4 laser (Millenia X, Spectra Physics), pulsing at a basic repetition rate of ~80 MHz was used. The pulse width was ~1 ps. The pulse repetition rate was decreased to 8 MHz using a pulse selector (model 3980, Spectra Physics). The fundamental 885 nm light was then frequency-tripled to 295 nm using a flexible second- and third-harmonic generator (GWU, Spectra Physics). The resultant 295 nm radiation was used as the excitation source and focused on the sample in the cuvette.

The fluorescence emission was passed through a monochromator (H10-UV, Horiba Jobin-Yvon) set at 360 nm (bandwidth of 30 nm) onto a cooled microchannel plate PMT (model 3809U-50, Hamamatsu) biased at −3000 V. Additionally, a 325 nm long-pass filter was used to reduce contributions from scattered excitation light from buffers and optical components. A polarizer (Glan-Thompson) in the emission arm was set at 54.7° (magic angle) to avoid polarization effects.

Single-photon counting measurements were triggered by a photodiode (APD110, Thor Laboratories) and measured using a TCSPC card (SPC-630, Becker-Hickl) via a preamplifier (Ortec). The time per channel was set to 48.8 ps for all measurements, except for experiments with Cys70-TNB in the region up to the unfolded baseline, where the time per channel was set to 12.2 ps for higher resolution.

The instrument response function was recorded with each measurement for deconvolution. This was measured using scattered light from a colloidal solution of nondairy coffee whitener and consistently yielded a full width at half-maximum of ~40 ps. The fluorescence lifetime of NATA (3.0 ns) in aqueous buffer was routinely recorded as a standard during each experiment. All decay transients were collected to a peak count of 20000 and up to 99.9% of completion.

For each set of TRFRET experiments, fluorescence intensity decay curves were recorded for both the unlabeled (donor-only protein) and the corresponding TNB-labeled protein (donor−acceptor protein), at increasing denaturant concentrations, on the same day. Measurements were taken in quick succession to reduce variations arising from instrumental instabilities.

Data Analysis. *Calculation of FRET Efficiency.* In an intramolecular FRET system, the efficiency of transfer of energy from a donor fluorophore to an acceptor (E) depends on the separation between the donor and acceptor on the molecule (R). The transfer efficiency can be measured experimentally and translated to intramolecular distances using Forster's equation:

$$E = 1 - \frac{\tau_{DA}}{\tau_D} = \left[1 + \left(\frac{R}{R_0}\right)^6\right]^{-1} \quad (1)$$

$$R = R_0\left(\frac{\tau_{DA}}{\tau_D - \tau_{DA}}\right)^{1/6} \quad (2)$$

The Forster's radius, R_0, in angstroms, was determined for each FRET pair using the following equation:

$$R_0 = 0.211[Q_D \times J(\lambda) \times \kappa^2 n^{-4}]^{1/6} \quad (3)$$

where Q_D is the quantum yield of the donor fluorescence, $J(\lambda)$ is the normalized overlap integral, κ^2 is the orientation factor, and n is the refractive index of the medium.

An average value of $^2/_3$ was used for κ^2. This value can be applied to FRET systems when it is assumed that both donor and acceptor probes are freely rotating on time scales faster than the fluorescence lifetimes. Such isotropic dynamic averaging is justified for the FRET pairs used in this study, and the use of a κ^2 of $^2/_3$ is based on the following observations. (1) The anisotropy decay kinetics of the donor W53 shows rapid depolarization of fluorescence [rotational correlation times of 0.15 ns (16%) and 5.5 ns (84%) in the native form and 0.21 ns (46%) and 2.8 ns (54%) in the unfolded form], indicating rapid averaging of orientations. Furthermore, the acceptor positions C17 and C70 are both solvent-exposed, and the attached acceptor (TNB) is also expected to be rapidly and freely rotating. (2) Experimentally determined R values from FRET agree with those measured from the NMR solution structure[39] after accounting for linker lengths (19.7 and 17.5 Å, compared to NMR structure values of 14.9 and 9.1 Å for W53−C17 and W53−C70 FRET pairs, respectively).

The values of R_0 for both the FRET pairs calculated independently in the N and U states are similar to each other (21.9 ± 0.4 Å) and to those reported previously for Cys17-TNB.[4] This also accounts for differences in the quantum yield of Trp and refractive index at high denaturant concentrations. Hence, it seems justified to assume it to be constant across the range of denaturant concentrations, and an average value of 22 Å was used for all distance measurements.

Changes in the fluorescence lifetimes of the donor in the unlabeled and labeled proteins, as determined by discrete analysis of fluorescence decay kinetics, can be directly translated to intramolecular donor−acceptor distances using the equations given above. For taking accurate distance measurements across a range of denaturant concentrations in the equilibrium unfolding transition, it is important that there is little variation in R_0 and τ_D between the N and U states.

Cys17 and Cys70 show similar lifetime values, as determined by discrete analysis for the single tryptophan residue (W53) in the native and GdnHCl-unfolded states. The lifetime values are also similar to that determined for the wild-type protein, which contains only the single tryptophan residue and no cysteine. The average lifetimes are different by 5−10% in 0 and 6 M GdnHCl. Urea has a strong effect on the fluorescence of the exposed tryptophan residue. The area under the spectrum changes by ~30%, as do the average lifetimes between the N state and the U state in 9 M urea. Even though τ_D is not constant across the entire range of denaturant concentrations, taking accurate distance measurements is still possible, because the corresponding donor lifetime at each denaturant concentration is used to calculate intramolecular distances.

Using the approximations described above, N-state distances for both donor−acceptor pairs were reliably recovered. This includes accounting for the contribution of the length of the TNB arm and the distance from the centers of the indole ring of tryptophan to the aromatic ring of TNB.

Discrete Analysis of Fluorescence Intensity Decays. The fluorescence intensity decays were deconvoluted with the IRF and analyzed as a sum of three (or four) exponentials:

$$I(t) = \sum_{i=1}^{3} \alpha_i e^{(-t/\tau_i)} \quad (4)$$

$$I(t) = \sum_{i=1}^{4} \alpha_i e^{(-t/\tau_i)} \quad (5)$$

dx.doi.org/10.1021/bi401337k | Biochemistry 2013, 52, 9482−9496

The mean lifetime, or the amplitude-average lifetime, was calculated as

$$\tau_m = \frac{\sum \alpha_i \tau_i}{\sum \alpha_i} \quad (6)$$

All the intensity decay curves were fit from the peak of the decay. This did not result in any loss of kinetic information; the observed mean lifetimes were found to be consistent with the measured steady-state intensities. Analysis from the rising edge of the decay gave poor fits to the data, presumably because of problems with the position of the IRF relative to the decay.[40]

MEM Analysis of Fluorescence Intensity Decays. Fluorescence intensity decays for the unlabeled (Cys17 only) and TNB-labeled mutant proteins were analyzed using a customized MEM analysis program.[34,35,41] MEM analysis is independent of any physical model or mathematical equation describing the distribution of lifetimes, which distinguishes it from other methods of analyzing fluorescence decays. The analysis begins with the assumption that the decay originates from a distribution of fluorescence lifetimes in the range from 10 ps to 10 ns (15 ns in some cases) or in a similar range and all lifetimes are equally probable (equal amplitude). The distribution is modified in subsequent iterations of the analysis to result in a minimization of the residuals and χ^2 values, and maximization of the Shannon–Jaynes' entropy, which is described as

$$S = -\sum p_i \log p_i \quad (7)$$

where p_i is the probability (amplitude) of the ith lifetime, defined as

$$p_i = \alpha_i / \sum \alpha_i \quad (8)$$

Analysis parameters were optimized for obtaining precise and reproducible MEM distributions. Care was taken to ensure that the distributions shown in this work are not limited by the signal-to-noise ratios. We have confirmed that the width reaches the limiting value when the peak count reaches ~20000. Also, peak resolution did not improve beyond a peak count of ~20000. Further increases in the count cause systematic errors resulting from laser instabilities.

The peak lifetime from each distribution was then estimated physically and averaged across traces. This was only possible for lifetime distributions in the native and unfolded protein baseline regions where peaks corresponding to the N-state or U-state lifetimes were clearly discernible. Because of the high degree of variability in the widths of the lifetime distributions, these could not be quantified.

A nonlinear, least-squares curve fitting algorithm in MATLAB was used to fit the fluorescence lifetime distributions according to a two-state model. The algorithm uses the spectra of the native $[N(\tau)]$ and unfolded $[U(\tau)]$-state fluorescence lifetime distributions as basis spectra and performs a global, least-squares fit of all the fluorescence lifetime distributions at all denaturant concentrations to the following equation:

$$y = f_N \times N(\tau) + f_U \times U(\tau) \quad (9)$$

where f_N and f_U represent the fractions of native and unfolded protein, respectively, at each denaturant concentration for the best possible global fit to the two-state model. This should ideally sum to 1.0 at all concentrations, but at certain intermediate denaturant concentrations, there is a deviation of 5–10%, most likely due to the lack of clear baselines for these lifetime distributions. The fraction that adds up the total to 1.0 is calculated $[\delta = 1 - (f_N + f_U)]$ and plotted along with the coefficients from the global fits. The analysis terminated when the sum of squares of errors (SSE) was less than a specified tolerance of 10^{-8}. The SSE was calculated as

$$\mathrm{SSE} = \sum [f(x, x_{data}) - y_{data}]^2 \quad (10)$$

where $f(x,x_{data})$ is the fitted data set and y_{data} is the experimentally observed data set. A small value of SSE indicates a satisfactory fit of the model to the data.

RESULTS

In this study, the intramolecular distance separating W53 from a thionitrobenzoate (TNB) label attached to C17 in one mutant variant (Cys17) of the PI3K SH3 domain, as well as that separating W53 from a TNB label attached to C70 in another mutant variant (Cys70), was individually monitored by FRET measurement. These two FRET pairs encompass distances from the center of the protein to nearly the N- and C-terminal ends of the polypeptide chain, and their measurement allows exploration of the intramolecular changes occurring between different structural elements in the protein, i.e., between a β-strand and a long loop region (W53–C17) in the labeled protein Cys17-TNB or a short loop region (W53–C70) in the labeled protein Cys70-TNB.

Equilibrium Unfolding Monitored by Steady-State Fluorescence. Figure 2 shows unfolding transitions monitored by tyrosine fluorescence at 300 nm. The PI3K SH3 domain has seven tyrosine residues distributed in space and sequence. The

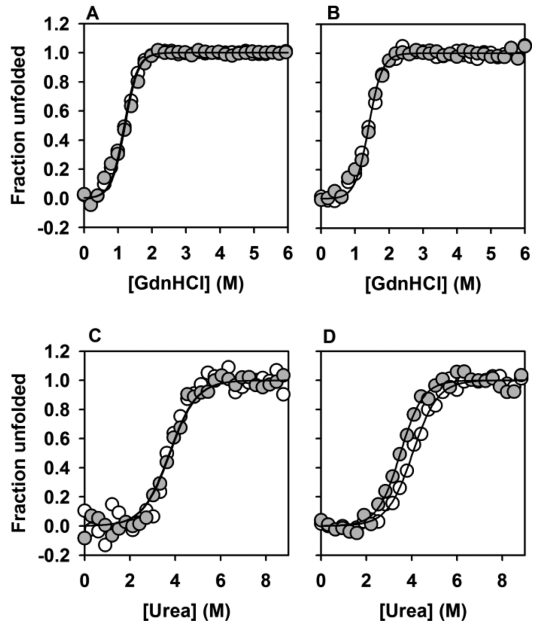

Figure 2. Stability of single-cysteine mutant proteins, Cys17 and Cys70, probed by monitoring tyrosine fluorescence at 300 nm. Equilibrium unfolding transitions in GdnHCl (A and B) and urea (C and D) were monitored for Cys17 (A and C) and Cys70 (B and D). White and gray circles indicate data for the unlabeled protein and the protein labeled with TNB, respectively. The solid black lines indicate sigmoidal nonlinear regression fits to a two-state unfolding model.[45] The C_m values obtained from the fits are 1.3 ± 0.1 M for unfolding transitions in GdnHCl and 3.7 ± 0.2 M for unfolding transitions in urea.

dx.doi.org/10.1021/bi401337k | *Biochemistry* 2013, 52, 9482–9496

Table 1. Fluorescence Lifetimes (τ_i) and Their Amplitudes (α_i) Obtained from Discrete Analysis of Fluorescence Intensity Decays[a]

protein		τ_1 (α_1) (ns)	τ_2 (α_2) (ns)	τ_3 (α_3) (ns)	τ_4 (α_4) (ns)	τ_m (ns)
Cys17	native	7.60 (0.16)	2.13 (0.34)	0.49 (0.51)	–	2.15
	GdnHCl	3.23 (0.42)	1.59 (0.37)	0.39 (0.22)	–	2.03
	urea	4.01 (0.62)	1.47 (0.30)	0.65 (0.15)	–	2.89
Cys17-TNB	native	6.03 (0.05)	1.13 (0.16)	0.24 (0.78)	–	0.67
	GdnHCl	3.14 (0.34)	1.50 (0.42)	0.37 (0.24)	–	1.80
	urea	3.89 (0.53)	1.61 (0.31)	0.36 (0.16)	–	2.59
Cys70	native	7.02 (0.19)	1.96 (0.34)	0.47 (0.47)	–	2.26
	GdnHCl	3.42 (0.32)	1.54 (0.39)	0.33 (0.25)	–	1.86
	urea	4.48 (0.44)	1.96 (0.36)	0.50 (0.19)	–	2.80
Cys70-TNB	native	6.64 (0.04)	1.70 (0.09)	0.40 (0.13)	0.07(0.74)	0.61
	GdnHCl	2.75 (0.29)	1.05 (0.43)	0.21 (0.29)	–	1.17
	urea	3.40 (0.26)	1.18 (0.41)	0.25 (0.32)	–	1.61

[a]Lifetimes for the unfolded states were measured in 4 M GdnHCl or 8 M urea. The mean lifetime was calculated as the amplitude-averaged lifetime. The error associated with each measurement was ~10−15%. More explicit values of errors are given in Figure 10.

probe therefore monitors global unfolding. The stabilities of Cys17 and Cys70 were measured before and after they had been labeled with TNB and appear to be similar to that of the wild-type protein, as reported in an earlier study.[2] This implies that the mutations and subsequent labeling do not significantly alter the structure or stability of the protein.

The tryptophan fluorescence emission spectrum displays a peak at 357 nm, which does not shift upon unfolding, or upon labeling with TNB (data not shown). This indicates that the W53 residue is completely solvent-exposed in the native (N) and unfolded (U) states of the protein. The fluorescence intensity of W53 in the unlabeled protein increases by ~30% upon unfolding in urea, which can be attributed to the solvent effect of urea on tryptophan fluorescence.[42] The lack of a single value of donor-alone fluorescence lifetime complicates FRET measurements taken in the time-resolved mode. TRFRET experiments reveal, however, similar trends in both denaturants, emphasizing the advantages of time-resolved measurements in FRET studies.

Time-Resolved Fluorescence Decays Are Required To Be Fit by a Sum of Exponentials. When the time-resolved tryptophan fluorescence decays were subject to discrete analysis (see Materials and Methods), it was found that they could be described as three- or four-exponential processes. Table 1 lists the individual lifetime components and their respective amplitudes recovered from discrete analysis of the fluorescence intensity decays of the unlabeled (Cys17 and Cys70) and TNB-labeled (Cys17-TNB and Cys70-TNB) proteins in the N and U states. For Cys17-TNB, the N-state decay is fit well only by the sum of three exponentials (eq 4), with the amplitude of the short lifetime being dominant. For Cys70-TNB, the N-state decay requires a sum of four lifetimes to be fit reliably (eq 5). Finally, the U states of both Cys17-TNB and Cys70-TNB show three lifetime components that are similar to those seen for unfolded Cys17 and Cys70.

TRFRET Measurement of the Mean Lifetime of Tryptophan Fluorescence Monitors the Equilibrium Unfolding Transition. Fluorescence intensity decays for W53 in the protein in different concentrations of denaturant, either guanidine hydrochloride (GdnHCl) or urea, were acquired, and each was fit to the sum of three or four exponentials (discrete analysis). Representative fluorescence decays are shown in Figure S1 of the Supporting Information, demonstrating the quality of the fits and the residuals for discrete analysis. Figure 3 shows the dependences on denaturant concentration of the mean fluorescence lifetime

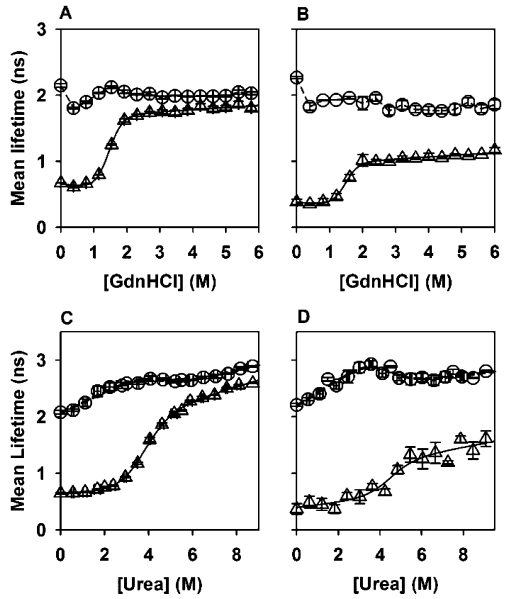

Figure 3. Unfolding transitions monitored by time-resolved fluorescence measurements. The mean excited-state lifetime of W53 in the absence (○) and presence (△) of FRET at each GdnHCl or urea concentration was calculated using eq 6. Data are shown for Cys17 in panels A and C and for Cys70 in panels B and D. Error bars are standard errors from two or three independent experiments. The solid lines through the data in the presence of FRET are nonlinear regression fits to a two-state unfolding model.[45] The dashed lines through the data in the absence of FRET have been drawn by inspection and do not represent fits.

(τ_m), which is the amplitude-averaged lifetime (see eq 6) and is proportional to the steady-state fluorescence intensity. As expected for the solvent-exposed W53, the values of τ_m for the two unlabeled proteins are very similar and do not change substantially at high denaturant concentrations. The extent of quenching of the N-state lifetime is different for Cys17-TNB and Cys70-TNB and is determined by the N-state distances. Also, the extent of the change in τ_m upon unfolding in GdnHCl and urea is different, with urea-induced unfolding showing a greater change than GdnHCl-induced unfolding. The mean

lifetime increases by 3−4-fold in Cys17-TNB and by 3-fold in Cys70-TNB, upon unfolding. This is indicative of a decrease in FRET efficiency, corresponding to an increase in the average D−A distance upon unfolding. Importantly, the midpoint (C_m) of the equilibrium unfolding curve of Cys17-TNB or Cys70-TNB was the same whether it was monitored by measurement of τ_m or by measurement of steady-state fluorescence intensity (data not shown).

Figure 4 shows FRET efficiencies and average D−A distances recovered from τ_m values at different denaturant concentrations, using eqs 1 and 2. For Cys17-TNB, the N-state FRET efficiency is nearly 70%, corresponding to an average D−A distance of 20 Å. For Cys70-TNB, the N-state FRET efficiency is nearly 80%, corresponding to an average D−A distance of ∼17 Å. The average W53−C17 and W53−C70 distances were found to be 31.4 and 24.0 Å, respectively, for Cys17-TNB and Cys70-TNB unfolded in 4 M GdnHCl and are, hence, significantly shorter than those expected from the random coil model (45.9 and 29.6 Å for W53−C17 and W53−C70 distances, respectively).[43] Similar observations have been made for the U states of other proteins.[44]

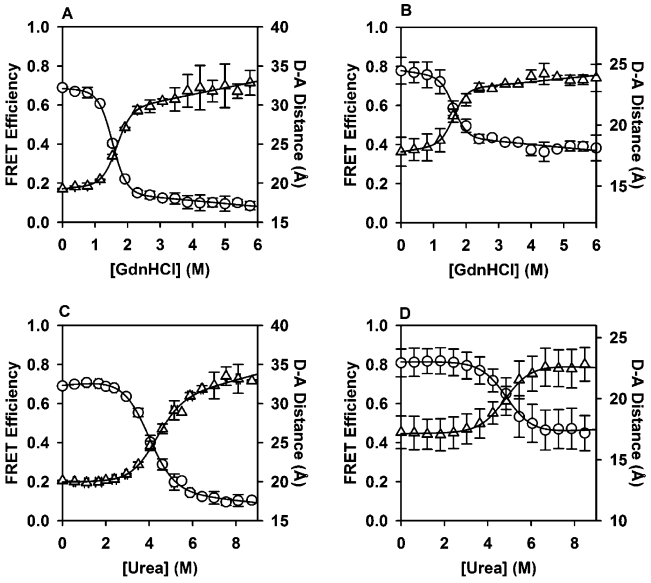

Figure 4. FRET efficiencies and average D−A distances from TRFRET measurements. The average energy transfer efficiencies (○) and the corresponding intramolecular distances (△) were obtained from discrete analysis of fluorescence intensity decays. FRET efficiencies were calculated using eq 1, and the corresponding distances were calculated using eq 2 and an R_0 of 22 Å. Data are shown for Cys17 in panels A and C and for Cys70 in panels B and D. The solid lines through the data are fits to a two-state unfolding model.[45] Error bars are standard deviations from two or three independent FRET experiments. The recovered native-state distances are 19.7 Å for the W53−C17 pair and 17.5 Å for the W53−C70 pair, in agreement with the expected distances measured using PyMol.

Measurement of the Individual Lifetime Components Reveals the Heterogeneity Inherent in the Equilibrium Unfolding Reaction. Figure 5 shows the dependences of the individual lifetime and amplitude components of Cys17, Cys17-TNB, Cys70, and Cys70-TNB on GdnHCl concentration. Similar trends are observed for the unfolding transitions in urea (data not shown). The key features of the changes in the individual lifetime and amplitude components in the presence of denaturant and upon addition of a TNB label are described below

Unlabeled Protein Lifetimes. Cys17 and Cys70 show very similar levels of heterogeneity in their lifetimes. This is expected in the absence of FRET, for which only the decay of W53 is monitored in each case.

The N state is unique in the appearance of a long lifetime component (τ_1) on the order of 7−8 ns (Figure 5A). While the amplitude of this component (α_1) in the N state is very small (Figure 5D), its contribution to τ_m or to the total fluorescence intensity (determined by $\alpha_i\tau_i$) is nearly 50%. The intermediate and short lifetime components are most similar to those seen for free L-tryptophan in solution (Figure 5B,C). Neither of these amplitudes is clearly dominant (α_2 = 35%, and α_3 = 50%), making it difficult to choose any one component as a single τ_D value for determining FRET efficiencies.

Three lifetime components persist in the U state, but their values change dramatically. The long lifetime component (τ_1) decreases from 7 to 3.5 ns in an apparent two-state transition (Figure 5A). The corresponding amplitude (α_1) increases more than 2-fold in the U state, keeping the contribution of this component to the total fluorescence intensity constant (Figure 5D).

The intermediate and short lifetime components (τ_2 and τ_3, respectively) show very small changes upon unfolding and do not show sigmoidal unfolding transitions (Figure 5B,C). In GdnHCl, the shapes of the lifetime transitions closely resemble those measured by steady-state tryptophan fluorescence, and this very likely represents the global unfolding transition (compare with Figure 3A,B). The respective amplitudes appear to undergo a transition in a two-state manner (Figure 5E,F).

Effect of Labeling on the Native Protein Lifetimes. In their N states, Cys17 and Cys70 show differences in the extents to which the different lifetime components change upon labeling Cys17-TNB and Cys70-TNB, respectively. Also, there is significant reshuffling of the amplitudes of the different lifetime components.

For Cys17-TNB, the long lifetime (τ_1) (Figure 5A) does not change significantly upon labeling, but its amplitude (α_1) (Figure 5D) decreases to <5%. The intermediate and short lifetimes both decrease by approximately half, indicating quenching by FRET (Figure 5B,C). The amplitude of the intermediate lifetime (α_2) (Figure 5E) also decreases to nearly 20%. These changes in amplitude are compensated for by an increase in the amplitude of the short lifetime component (α_3) (Figure 5F) that increases to nearly 80%, making this the dominant lifetime component in the N state of Cys17-TNB.

For Cys70-TNB, the decay traces for the N state and at low denaturant concentrations, up to the C_m, fit significantly better to a four-exponential equation than to a three-exponential equation (Figure 5G−N). A dominant (80% amplitude) component in the range of 50−70 ps is seen (τ_4) (Figure 5J). While the long and short lifetime components (τ_1 and τ_4, respectively) (Figure 5G,J) fall in ranges set by Cys70, the intermediate lifetime component appears to be split into two (τ_2 and τ_3, respectively) (Figure 5H,I), with small differences in the lifetime values and their amplitudes. Decay kinetics for points beyond the C_m could be satisfactorily fit to a three-exponential equation.

GdnHCl-Induced Unfolding Transitions of TNB-Labeled Mutant Proteins. Upon unfolding, all the lifetime and amplitude components observed for both Cys17-TNB and Cys70-TNB appear to converge to the values seen for unfolded

dx.doi.org/10.1021/bi401337k | Biochemistry 2013, 52, 9482−9496

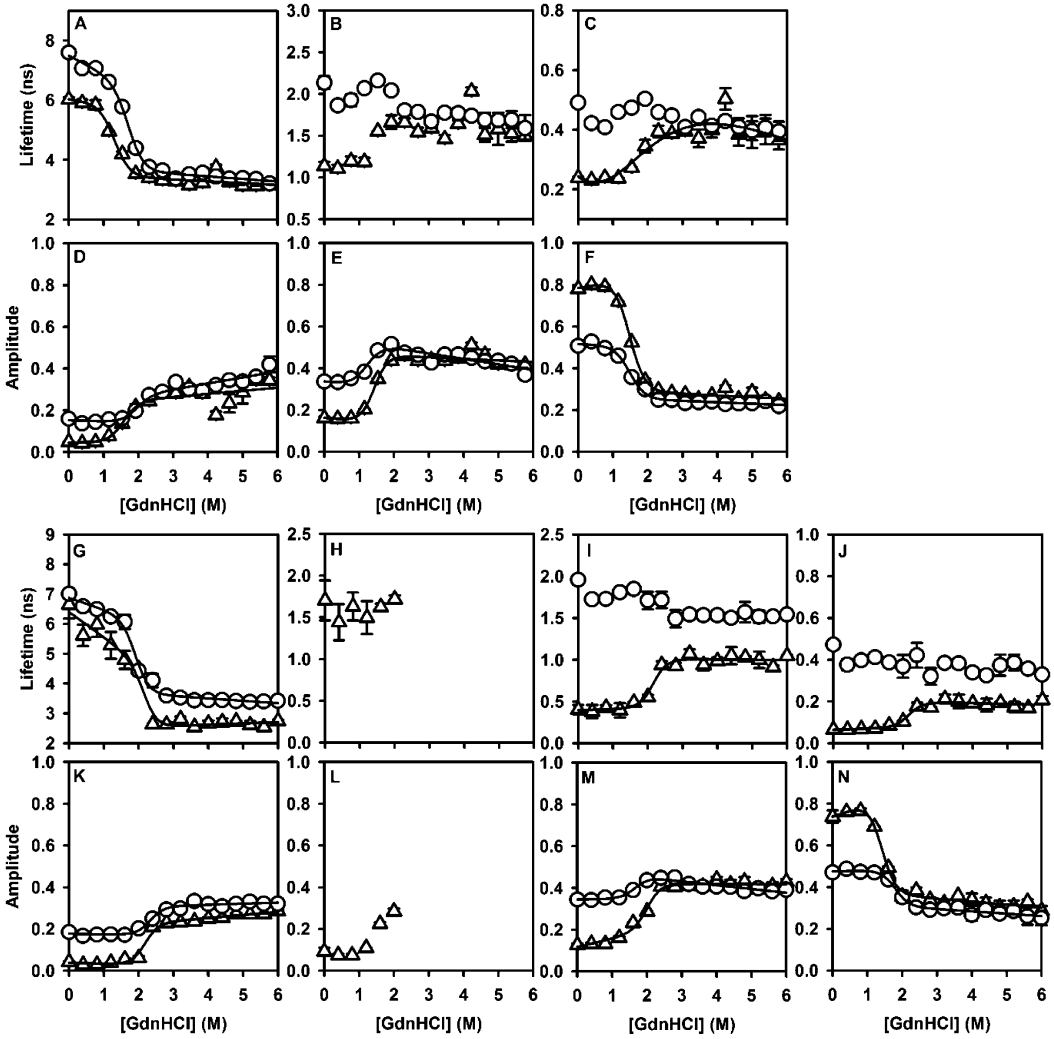

Figure 5. Time-resolved fluorescence-monitored unfolding in GdnHCl. The fluorescence decay curve at each denaturant concentration was fit to eq 4 or 5. Panels A–C (for Cys17) and G–J (for Cys70) show the lifetime components for the donor fluorescence decay curve for Cys17 and Cys70 (○) and for Cys17-TNB and Cys70-TNB (△). Panels D–F (for Cys17 and Cys17-TNB) and K–N (for Cys70 and Cys70-TNB) show the corresponding relative amplitudes for each component. Error bars are standard errors from two or three independent experiments. The solid lines are fits to a two-state unfolding model.[45] Data in panels B, C, I, and J (○) could not be fit to a two-state unfolding model.

Cys17 and Cys70. This suggests that upon release of energy transfer at high denaturant concentrations, the different forms are present as an apparently uniform U-state ensemble, in the cases of both Cys17-TNB and Cys70-TNB. Additionally, the lifetime and amplitude components display sigmoidal transitions in going from the N to the U state, suggesting cooperative unfolding transitions for each of these components.

In the case of Cys70-TNB, the shortest lifetime component ($\tau_4 \sim 0.07$ ns) disappears toward the end of the unfolding transition. This prevents a direct analysis of the denaturant-dependent transition of τ_4 by a two-state model. Interestingly, the unfolded state of Cys70-TNB is still considerably quenched by TNB. Nearly 50% FRET efficiency is seen at high denaturant concentrations. From Figure 5, it appears that this quenching is a result of low values of the intermediate and short lifetime components, and not from any major difference in their amplitudes, with respect to unfolded Cys70. This is clearly in contrast to Cys17-TNB, for which both the lifetimes and the amplitudes approach those of unfolded Cys17.

Cooperative and/or Sigmoidal Dependences of Individual Lifetime and Amplitude Components on Denaturant Concentration Are Noncoincident. Table 2 lists the C_m values for the unfolding transitions recovered from fitting a two-state unfolding model[45] to the unfolding transitions of individual lifetime and amplitude components in Figure 5. These are also compared to the midpoints of the unfolding transitions monitored by mean lifetime, tyrosine fluorescence, and average FRET efficiency, which were also similarly fit. All lifetime and amplitude components that show a significant change (≥2-fold) between the N and U states have a sigmoidal dependence on denaturant concentration, which could be fit to this model. Components that did not show a cooperative transition or changed by <1.5-fold upon unfolding could not be fit. For most of the transitions, there are only a few points spanning the transition zone and the slopes of the native and unfolded protein baselines are steep. Despite this, the fits returned satisfactory regression coefficient values (>0.85), and the errors associated with fitting were small.

The C_m values obtained by ensemble-averaging measurements, i.e., mean lifetime and tyrosine fluorescence, are quite similar (standard deviation of ±0.2 M in GdnHCl) (Table 2). In contrast, C_m values of the individual lifetime and amplitude

dx.doi.org/10.1021/bi401337k | *Biochemistry* 2013, 52, 9482–9496

Table 2. Denaturation Midpoints of the Equilibrium Unfolding Transitions in GdnHCl[a]

	C_m for GdnHCl-induced unfolding transitions (M)			
	Cys17	Cys17-TNB	Cys70	Cys70-TNB
τ_1	1.8	1.2	1.9	2.2
τ_2	–	–	–	–
τ_3	–	1.8	–	2.2
τ_4	–	–	–	2.2
α_1	2.0	1.6	2.3	2.2
α_2	1.3	1.5	1.7	–
α_3	1.3	1.5	1.8	2.0
α_4	–	–	–	1.4
mean W53 lifetime	–	1.4	–	1.6
tyrosine fluorescence	1.2	1.2	1.4	1.4
average FRET efficiency	–	1.5	–	1.5

[a]The unfolding transition for each lifetime and amplitude component was fit to a six-parameter equation derived for a two-state unfolding model. C_m values could not be measured in cases where the transitions were not clearly sigmoidal. Depending on the final signal change in the equilibrium unfolding transition, the uncertainties in measuring the C_m values varied between 10 and 20%.

components show significant dispersion, exceeding ±0.2 M. For most of these transitions, the individual lifetime or amplitude component shows a higher C_m value than does the corresponding ensemble-averaging probe. All these features indicate that the unfolding transitions of the individual lifetime and amplitude components are noncoincident. This is presumably a manifestation of the underlying conformational heterogeneity in the protein.

MEM Analysis of Time-Resolved Fluorescence Decays of the Unlabeled Protein. Figure 6 shows fluorescence lifetime distributions obtained for Cys17 at different GdnHCl (Figure 6A) and urea (Figure 6B) concentrations, from MEM analysis of the fluorescence decay curves. These distributions are broad and encompass lifetimes corresponding to those obtained by discrete analysis (Table 1). Although there is an apparent shift in the peak lifetimes with an increase in denaturant concentration, the area under the distribution, which represents total fluorescence intensity, remains nearly constant in the case of GdnHCl-induced unfolding but increases by ~40% in urea. This increase can be attributed to the solvent effect of urea on tryptophan fluorescence (see above). In the absence of a single, dominating lifetime component in the unlabeled (donor-alone) proteins, a single value of τ_D could not be applied to translate the fluorescence lifetime distributions of Cys17-TNB and Cys70-TNB into corresponding distance distributions.

An interesting observation of the fluorescence lifetime distributions of both Cys17 and Cys70 is that the N-state distributions are significantly broader than the U-state distributions. This is in contrast to studies with barstar, in which the N-state distributions at pH 7.0 are sharp and narrow and the U-state distributions are broad.[46,47] The increase in the width of the fluorescence lifetime distributions upon unfolding was consistent with the change from the rigid, compact environment of the buried tryptophan residue in the N state to a more flexible, solvent-accessible environment in the U state.[46,47] The width of a fluorescence lifetime distribution has been considered as a qualitative measure of the conformational heterogeneity in an ensemble. In the case of the PI3K SH3 domain, the widths appear to decrease with an increase in denaturant concentration, contrary to the assumption that conformational flexibility increases upon unfolding.

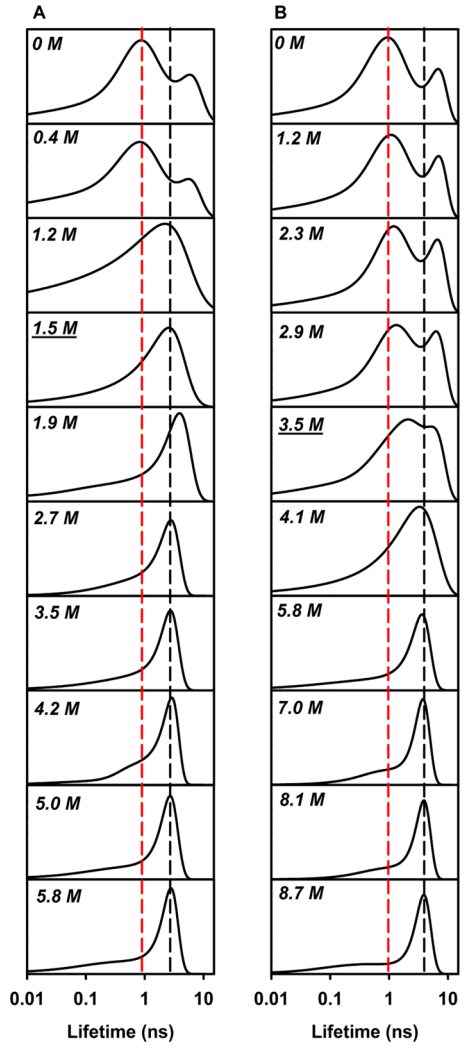

Figure 6. Equilibrium unfolding monitored by the evolution of the fluorescence lifetime distributions of Cys17. Panels A and B show the MEM-derived lifetime distributions for GdnHCl-induced and urea-induced unfolding, respectively, as a function of the denaturant concentration indicated at the top left of each panel. Fluorescence lifetime distributions at the denaturant concentration corresponding to the midpoint of the unfolding transition are indicated by underlining the C_m concentration. The *x*-axis is plotted on a log scale, while the *y*-axis units are arbitrary. The dashed red lines indicate the peak position of the N state, and the dashed black lines indicate the peak position of the U state in 4 M GdnHCl (A) and 8 M urea (B).

MEM Analysis of TRFRET-Monitored Unfolding. Figures 7 and 8 show the evolution of fluorescence lifetime distributions during unfolding in GdnHCl and urea, respectively, for Cys17-TNB and Cys70-TNB. Representative traces, showing the quality of the fits and residuals for MEM analysis, are shown in Figures S2 and S3 of the Supporting Information for GdnHCl- and urea-induced unfolding transitions, respectively. For both proteins, the lifetime distribution in the N state is nearly unimodal. The peak of the N-state distribution for each mutant protein corresponds closely with the dominant short lifetime component (Table 1), and the area under the distribution matches the mean lifetime obtained from discrete analysis. Fluorescence lifetime distributions of the TNB-labeled

dx.doi.org/10.1021/bi401337k | *Biochemistry* 2013, 52, 9482−9496

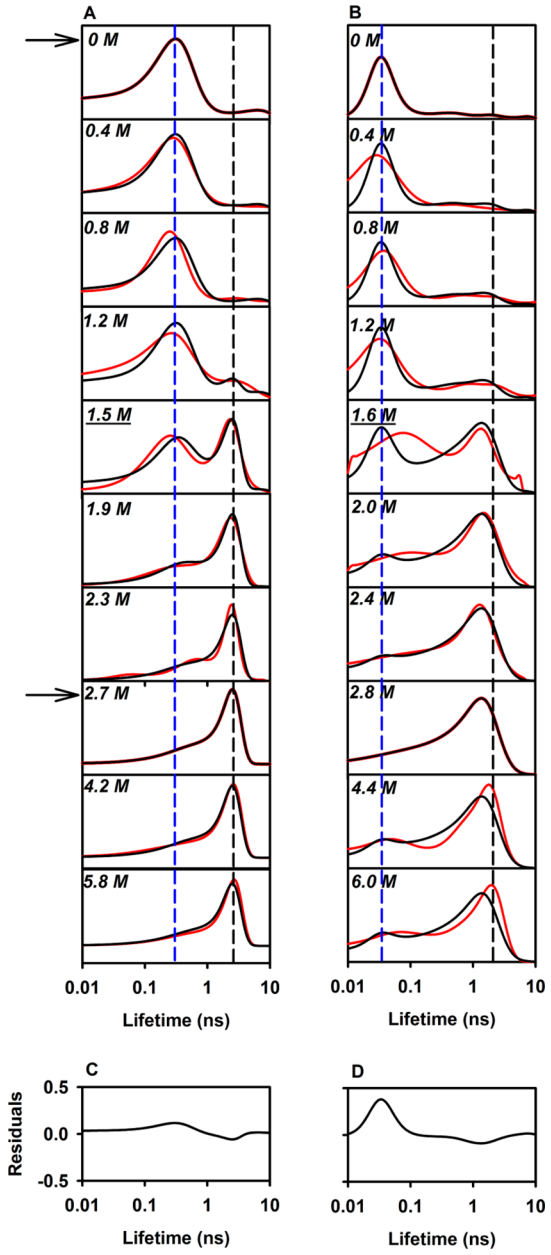

Figure 7. Equilibrium unfolding in GdnHCl monitored by the evolution of the fluorescence lifetime distributions of Cys17-TNB (A) and Cys70-TNB (B). The MEM-derived fluorescence lifetime distributions at all denaturant concentrations (indicated at the top left of each panel) were fit globally to a linear sum of native $[N(\tau)]$ and unfolded $[U(\tau)]$ fluorescence lifetime distributions (eq 9). The solid red lines indicate experimentally determined distributions, and the solid black lines indicate distributions obtained from the global fits to a two-state model. The arrows indicate the fluorescence lifetime distributions used as the native and unfolded protein basis spectra. In each of the four panels showing the basis distributions for N and U, the observed distribution in red falls exactly below the black line. The dashed blue and dashed black lines indicate the position of the N-state and U-state lifetimes, respectively. The *x*-axis is plotted on a log scale, while the *y*-axis units are arbitrary. Panels C and D show the residuals obtained from the two-state global fits.

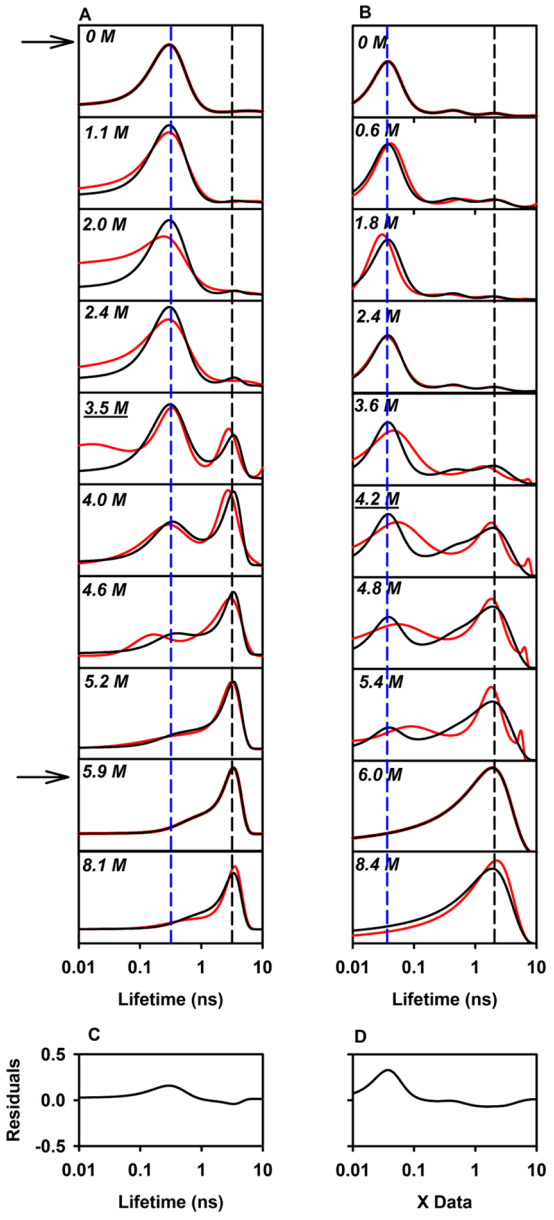

Figure 8. Equilibrium unfolding in urea monitored by the evolution of the fluorescence lifetime distributions of the TNB-labeled proteins: (A) Cys17-TNB and (B) Cys70-TNB. The MEM-derived fluorescence lifetime distributions at all denaturant concentrations (indicated at the top left of each panel) were fit globally to a linear sum of native $[N(\tau)]$ and unfolded $[U(\tau)]$ fluorescence lifetime distributions (eq 9). The solid red lines indicate experimentally determined distributions, and the solid black lines indicate distributions obtained from the global fits to a two-state model. The arrows indicate the fluorescence lifetime distributions used as the native and unfolded protein basis spectra. In each of the four panels showing the basis distributions for the N and U states, the observed distribution in red falls exactly below the black line. The dashed blue and dashed black lines indicate the position of the N-state and U-state lifetimes, respectively. The *x*-axis is plotted on a log scale, while the *y*-axis units are arbitrary. Panels C and D show the residuals from the two-state global fits.

proteins are mainly controlled by FRET. The main change in the lifetime distributions of the TNB-labeled proteins is a dramatic shift to a single peak centered on a short lifetime value. Such a decrease in fluorescence lifetime distributions in the presence of an acceptor is thus clearly linked to FRET. Thus, the evolution of these lifetime distributions as a function of denaturant concentration can be interpreted as evidence of increasing intramolecular distances, and structural transitions in the protein during unfolding.

dx.doi.org/10.1021/bi401337k | *Biochemistry* 2013, 52, 9482−9496

In the native baseline region, the peak position shows a measurable change for Cys70-TNB but not for Cys17-TNB. At denaturant concentrations spanning the transition region (0−1.5 M GdnHCl or 0−3.6 M urea), the lifetime distribution becomes bimodal, with the appearance of two peaks corresponding to N- and U-state lifetime distributions, respectively. This may seem to be evidence of a two-state unfolding model, where, at C_m, only the N and U states are populated to equal levels (but see later). At denaturant concentrations spanning the unfolded protein baseline region, the lifetime distributions are once again unimodal. For both structural segments being probed, the peak position and, hence, the intramolecular distances appear to increase with an increase in denaturant concentration in the unfolded baseline region.

Inadequacy of the Two-State Model in Fitting Fluorescence Lifetime Distributions. The evolution of fluorescence lifetime distributions for each mutant protein was quantitatively analyzed in terms of a two-state equilibrium unfolding model.[45] The analysis involved performing a global, least-squares fit of all the fluorescence lifetime distributions for each mutant protein to a model that assumes that each distribution could be described as a linear sum of native and unfolded protein fluorescence lifetime distributions.

Figures 7 and 8 also compare the experimentally determined fluorescence lifetime distributions, with distributions simulated for a two-state model. The goodness of fit for the global fits was determined by the residuals from the global analysis (Figures 7C,D and 8C,D) and a visual comparison of observed and simulated lifetime distributions. Although the model appears to describe the data reasonably well for Cys17-TNB (Figures 7A and 8A), the simulated distributions show significant deviations from the experimentally observed distributions in the case of Cys70-TNB (Figures 7B and 8B). This is also clearly seen from the distribution of the residuals for both mutant proteins (Figures 7C,D and 8C,D). This implies that a two-state model is inadequate for describing the equilibrium unfolding transition of the PI3K SH3 domain.

The simulated values of the fraction of N-like and U-like forms determined by the global fit were also analyzed according to a two-state model, and this is shown in Figure 9. The midpoints of these equilibrium unfolding transitions were similar to those measured from τ_m measurements, although deviations on the order of 0.3−0.5 M were observed in the case of Cys70-TNB unfolding in urea. While this has not been presented in Table 2 for the sake of clarity, the C_m of the unfolding transition when measured using the mean lifetime of W53 was 4.5 M urea, using tyrosine fluorescence was 3.5 M urea, and as predicted by the two-state model was 4.1 M urea. These deviations indicate that there are site-specific differences in the unfolding transitions of different segments of the protein and reinforce the inadequacy of a strictly two-state unfolding model.

Structural Changes in the N and U States. Peak lifetime values from MEM-derived distributions were compared with results from discrete analysis (Figure 10). As mentioned earlier, the trends in both GdnHCl (Figure 10A−F) and urea (Figure 10G−L) are observed to be similar. While it is more common to use the area under the lifetime distributions as an indicator of mean lifetime or average fluorescence intensity, the lack of reproducibility in determining the widths of these distributions in this particular case makes it difficult to quantify areas accurately. When measurements are taken on mixtures of (two or three) noninteracting dyes, the peak values from the lifetime

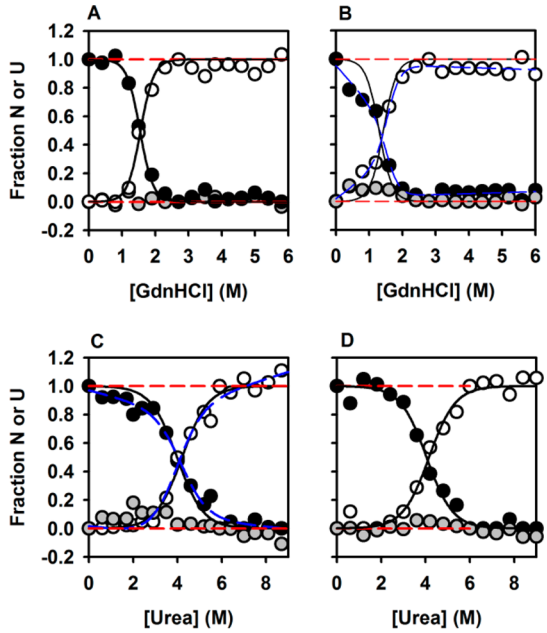

Figure 9. Equilibrium unfolding transitions obtained from simulated global fits for a two-state model. The fraction native (●), fraction unfolded (○), and a small remaining fraction (gray circles), resulting from incomplete baseline selection, obtained from global fits of the MEM-derived lifetime distributions (Figures 7 and 8) were plotted as a function of GdnHCl (A and B) and urea (C and D) concentration. Data are shown for Cys17-TNB (A and C) and Cys70-TNB (B and D). The solid black lines are fits to a two-state unfolding model.[45] The dashed blue lines in panels B and C are fits to a six-parameter equation for a two-state unfolding model.[45] Both fits yield C_m values similar to those obtained from mean lifetime measurements, but slightly lower for the unfolding of Cys70-TNB in urea. These values are 1.5 M for Cys17-TNB and 1.4 M for Cys70-TNB for the unfolding transitions in GdnHCl and 3.9 M for Cys17-TNB and 4.1 M for Cys70-TNB for unfolding transitions in urea.

distributions are found to match those obtained from discrete analysis (data not shown). In the case of the PI3K SH3 domain, the peak value obtained from the lifetime distribution agrees with those obtained from discrete analysis (sum of two or three exponentials) and the areas under the individual distributions match with the relative amplitudes obtained in discrete analysis (data not shown). Thus, this comparison shows similar trends from both methods of analysis, suggesting that the peak lifetime values can be used as a suitable proxy for indicating structural changes from fluorescence lifetime distributions.

For both Cys17-TNB and Cys70-TNB, the peak lifetimes at denaturant concentrations in the native protein baseline region of the equilibrium unfolding curve correspond to the short lifetime components obtained from discrete analysis. This equivalence between the results from discrete and MEM analysis is important to demonstrate that the changes in the fluorescence lifetime distributions obtained from MEM analysis can reflect the structural transitions observed during unfolding. While the N-like lifetimes show no evidence of increasing distances at low denaturant concentrations in the case of Cys17-TNB (Figure 10B,H), the lifetime of the N state of Cys70-TNB increases (Figure 10E,K) by a factor of nearly 2 in the native protein baseline region (0−1.5 M GdnHCl or 0−4 M urea), with a linear dependence on denaturant concentration. This indicates that the N state expands progressively, at

dx.doi.org/10.1021/bi401337k | Biochemistry 2013, 52, 9482−9496

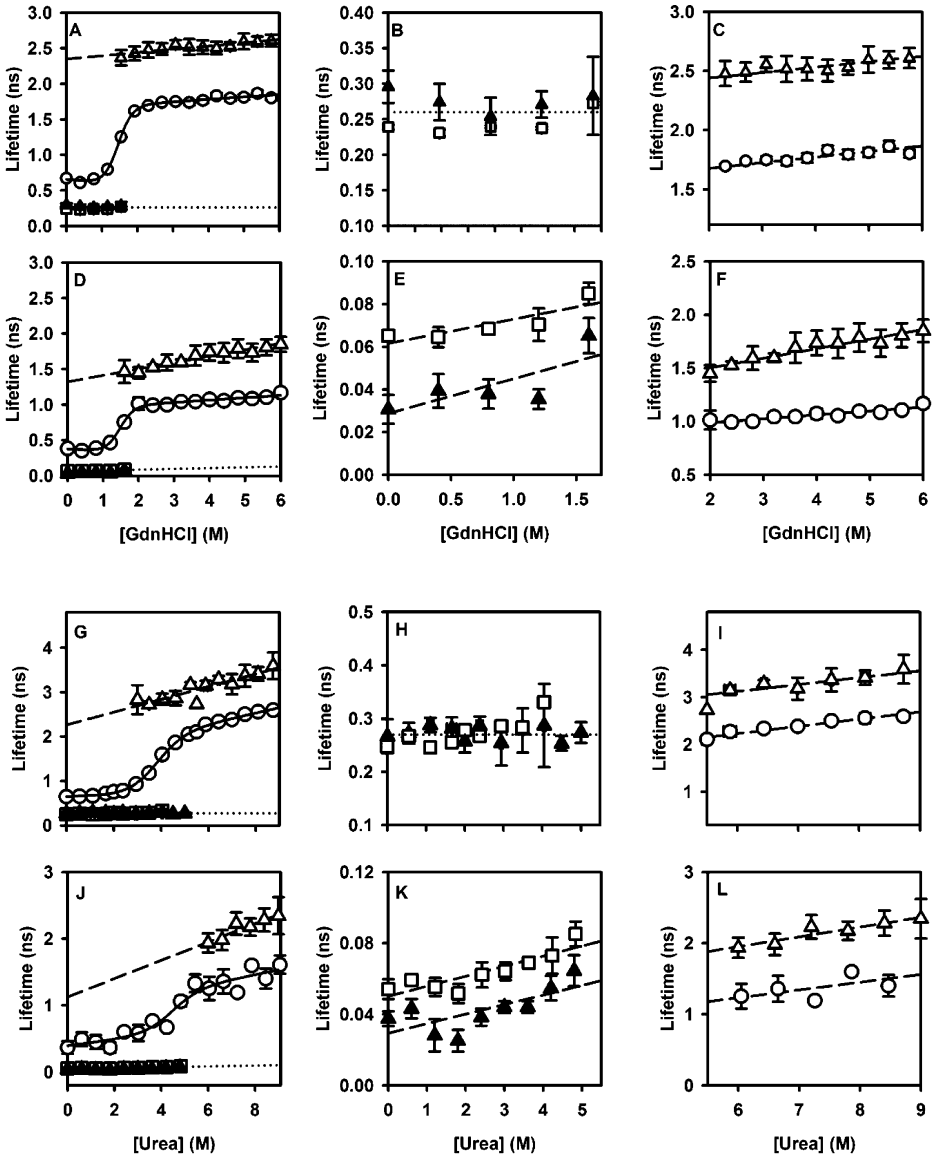

Figure 10. Analysis of peak lifetimes obtained from MEM analysis and mean lifetimes obtained from discrete analysis of fluorescence decays measured in the equilibrium unfolding experiments. Data for experiments in GdnHCl are shown in panels A–F, and data for experiments in urea are shown in panels G–L. For Cys17-TNB (A–C and G–I) and Cys70-TNB (D–F and J–L), the peak values obtained from MEM analysis-derived fluorescence lifetime distributions are shown for the native protein baseline (▲) and unfolded baseline (△) regions of the equilibrium unfolding curves. These are compared against the mean lifetime (○) and the shortest lifetime component (□) obtained by discrete analysis. The solid black lines in panels A, D, G, and J are fits to a two-state unfolding model.[45] The dashed lines in all panels are fits to a linear equation. The dotted lines in panels A, B, D, G, H, and J were drawn by inspection.

least in this segment of the structure, under increasingly destabilizing conditions.

In the unfolded protein baseline region, both Cys17-TNB and Cys70-TNB show evidence of swelling with an increasing denaturant concentration, as seen from the increase in the values of both the peak position and the mean lifetime. Values of the dependences on denaturant concentration obtained from both peak lifetimes (from lifetime distributions obtained by MEM analysis) and mean lifetimes (from discrete analysis) are shown in Figure 10.

■ DISCUSSION

The main aim of this work was to critically evaluate the validity of the commonly used two-state model for equilibrium protein folding–unfolding transitions, using the PI3K SH3 domain as a model protein. FRET between two intramolecular distances was monitored during equilibrium unfolding. Time-resolved fluorescence was analyzed by both discrete analysis and model-free MEM analysis. The strengths and weaknesses of both these methods in addressing questions of conformational heterogeneity in proteins are examined.

Discrete Analysis and Conformational Heterogeneity. Unlabeled and TNB-labeled mutant proteins show three or four fluorescence lifetimes for W53, upon analysis by a discrete model (Table 1). The common interpretation of such an observation is to correlate the individual lifetime components with population heterogeneity, originating mainly from χ^1 (C_α–C_β) and χ^2 (C_β–C_γ) rotamers of the Trp indole group,[41,48–50] as well as from other structural features.[50–52]

dx.doi.org/10.1021/bi401337k | *Biochemistry* 2013, 52, 9482–9496

Although both the N and U forms show three (and in some cases four) lifetimes, the values of the lifetimes and their amplitudes are quite different from each other (Table 1). In this scenario, a set of six (or more) correlated parameters in the transition between the N and U states is obtained. Often, the inability to resolve these lifetime and amplitude components accurately results in the mixing of lifetime components and leads to perplexing results in which the observed values of lifetimes change continuously during the transition (Figure 5).

It is tempting to interpret the significant dispersion in the C_m values (Table 2) as an indication of folding−unfolding transitions that go beyond the minimal two-state model, with both the native and unfolded states being composed of substates that can be distinguished by their fluorescence lifetimes. However, caution should be exercised in view of the experimental inability to extract discrete fluorescence lifetimes associated with the N and U states reliably segregated from each other during the unfolding transition. Although such segregation could be partially achieved in some cases,[53,54] the complexity associated with the excited-state lifetimes of tryptophan has proven to be challenging in many other model systems.[55,56]

The unsuitability of discrete analysis methods can also be determined by (i) the observation of significant changes in the relative amplitudes of the three lifetime components following labeling with TNB (and, hence, FRET) in both the N and U states (Table 1) (if the three lifetime components were to arise from three discrete ground-state populations, FRET would not expected to cause any change in the relative amplitudes of these components), (ii) the estimation of intramolecular distances using the three individual lifetime components returning varying and incongruent values (data not shown), and (iii) bimolecular quenching constants for each of these components, measured by acrylamide and KI quenching, that varied by a factor of 10, which is unlikely for a case in which the Trp residue is completely solvent-exposed in each subpopulation (data not shown).

The limitations associated with discrete analysis are largely overcome by fluorescence lifetime distribution analysis especially using MEM.

Distribution Analysis by MEM Reveals That Equilibrium Unfolding Is "Beyond the Two-State Model". A key feature of using MEM analysis to generate the fluorescence lifetime distributions is the underlying model-free approach. This is unlike the use of Gaussian or Lorentzian distributions, in which both the shape and the number of peaks are preassigned.[56,57] A comparison of MEM-analyzed fluorescence lifetime distribution profiles (Figures 6−8) with fluorescence lifetimes obtained from discrete analysis (Table 1 and Figure 5) reveals the lack of a clear correlation in terms of peak positions in the distributions corresponding to the discrete lifetime components. Thus, the observation of continuous changes in lifetime values obtained using discrete analysis during denaturation (Figure 5) is inconsistent with results from MEM analysis (Figure 7). This reinforces the view that lifetime components obtained from discrete analysis do not correspond to discrete populations and that the recovered parameters are merely a result of mathematical fitting of decay kinetics. It is to be stressed that this cautionary note is pertinent, in general, to the analysis of the time-resolved fluorescence of complex systems, including proteins and nucleic acids. The observed broad distribution of lifetimes demands a model that extends beyond the popular "rotamer" model of tryptophan ground-state heterogeneity. It is likely that the large number of protein microstates sensed by the surface-exposed and flexible W53, coupled to the rotamer populations, results in the broad fluorescence lifetime distributions observed here. This also necessitates that there is slow interconversion between the microstates compared to the excited-state lifetime time scales (approximately nanoseconds). The relatively narrower distribution observed for the U state when compared to that for the N state (Figure 6) could be due to the abolition of multiple microstates of the N state as well as more rapid interconversion between various microstates in the U state of the protein. This observation is more prominent in the unlabeled protein where the fluorescence lifetime is controlled by a variety of unidentified nonradiative processes. A contrasting result is generally obtained when the tryptophan is buried and tightly packed in the protein core. In this situation, the N state is associated with a narrower distribution in comparison to that in the U state, as observed in the case of barstar[46,47] and other proteins.[41]

Fluorescence lifetime distributions in the TNB-labeled proteins (Figures 7 and 8) provide more information because they can be directly correlated with intramolecular distance distributions. The observation that TNB labeling drastically shifts lifetime distributions to shorter values confirms that FRET is the dominant factor controlling fluorescence lifetime distributions in the TNB-labeled proteins. Equilibrium unfolding appears to be bimodal with the distributions corresponding to N and U states well separated from each other (Figures 7 and 8). Rigorous analysis reveals, however, the unsuitability of a two-state equilibrium unfolding model, as seen from the nonrandom residuals obtained from fitting simulated two-state distributions (panels C and D of Figures 7 and 8). This result is a strong indicator of the requirement of a model more complex than a two-state model for describing the equilibrium unfolding of this protein. This is in contrast to a similar TRFRET-based study with BDPA,[56] in which the two-state model of equilibrium unfolding was based on obtaining a statistically better description of the intramolecular distance distribution for a two-subpopulation model, compared to a single-population model, at the C_m of the equilibrium unfolding transition for a single FRET pair. However, this work made an assumption about the existence of only two populations, and the analysis was not extended to test for the presence of multiple populations or more complexity in structural transitions.

In this study with the PI3K SH3 domain, lifetime distributions obtained using MEM analysis show directly, without making any assumptions about the nature of the equilibrium unfolding transition, that the distributions are unimodal for the N and U states and bimodal at the C_m. Further, by extending the analysis to multiple FRET pairs and testing the two-state model over the entire evolution of lifetime distributions, we could also show that the methodology based on MEM analysis-derived lifetime distributions can be used as a rigorous test for the validity of this model for equilibrium unfolding.

MEM analysis-derived fluorescence lifetime distributions also reveal structural transitions occurring both before and after the major N ↔ U transition. Expansion of the N state of Cys70-TNB at low denaturant concentrations (Figure 10E,K) is similar to that seen in the case of barstar.[8] This indicates continuous swelling of the N state prior to the main unfolding event. The fact that a similar expansion is not observed for

Cys17-TNB (Figure 10B,H) is again an indication of noncooperativity in the unfolding transition. The key differences between the two FRET pairs are based on the shorter intramolecular distance of the W53−C70 FRET pair, as well as the location of C70 (Figure 1). Expansion of the U state at high denaturant concentrations is reflected in the linear increase in the FRET-controlled fluorescence lifetimes of both Cys17-TNB and Cys70-TNB (Figure 10C,F,I,L) and presumably originates from solvent-driven expansion of the unfolded polypeptide.[44,58,59] Although an increase in denaturant concentration could be seen as a change from "bad" to "good" solvent, resulting in expansion of the unfolded polypeptide as expected from polymer theory,[60−63] abolition of residual structure leading to expansion cannot be ruled out.

CONCLUSIONS

In this study, multisite TRFRET measurements with the PI3K SH3 domain have shown that (i) multiple lifetime and amplitude components are seen in discrete analysis and suggest complex conformational heterogeneity, (ii) the evolution of intramolecular distances during equilibrium unfolding is better studied by generating fluorescence lifetime distributions using MEM, and (iii) site-specific differences in the equilibrium unfolding, such as in the expansion of the native state at low denaturant concentrations, indicate that the equilibrium unfolding transition of the PI3K SH3 domain cannot be described by a simple, two-state model. The results indicate the presence of several intermediates or a series of intermediates between the native and unfolded states. This study stresses the importance of comprehensive analysis of TRFRET measurements in the study of complex macromolecular systems such as proteins.

ASSOCIATED CONTENT

Supporting Information

Representative time-resolved fluorescence decays, quality of fits to discrete and MEM analysis methods, and the corresponding residuals (Figures S1−S3). This material is available free of charge via the Internet at http://pubs.acs.org.

AUTHOR INFORMATION

Corresponding Authors

*E-mail: gk@tifr.res.in. Telephone: 91-22-2278-2301.
*E-mail: jayant@ncbs.res.in. Telephone: 91-80-23666150. Fax: 91-80-23636662.

Funding

This work was funded by the Tata Institute of Fundamental Research and by the Department of Science and Technology, Government of India. G.K. and J.B.U. are recipients of J. C. Bose National Research Fellowships from the Government of India.

Notes

The authors declare no competing financial interest.

ACKNOWLEDGMENTS

We thank N. Periasamy for the MEM software and advice on its use, Saswata Sarkar for discussions, and M. H. Kombrabail for experimental assistance. We thank Erix A. Milán-Garcés for the use of the MATLAB program for two-state model analysis.

REFERENCES

(1) Mayer, B. J. (2001) SH3 domains: Complexity in moderation. *J. Cell Sci. 114*, 1253−1263.
(2) Wani, A. H., and Udgaonkar, J. B. (2009) Revealing a concealed intermediate that forms after the rate-limiting step of refolding of the SH3 domain of PI3 kinase. *J. Mol. Biol. 387*, 348−362.
(3) Dasgupta, A., and Udgaonkar, J. B. (2012) Four-state folding of a SH3 domain: Salt-induced modulation of the stabilities of the intermediates and native state. *Biochemistry 51*, 4723−4734.
(4) Dasgupta, A., and Udgaonkar, J. B. (2010) Evidence for initial non-specific polypeptide chain collapse during the refolding of the SH3 domain of PI3 kinase. *J. Mol. Biol. 403*, 430−445.
(5) Wani, A. H., and Udgaonkar, J. B. (2009) Native state dynamics drive the unfolding of the SH3 domain of PI3 kinase at high denaturant concentration. *Proc. Natl. Acad. Sci. U.S.A. 106*, 20711−20716.
(6) Dasgupta, A., and Udgaonkar, J. B. (2012) Transient non-native burial of a Trp residue occurs initially during the unfolding of a SH3 domain. *Biochemistry 51*, 8226−8234.
(7) Guijarro, J. I., Morton, C. J., Plaxco, K. W., Campbell, I. D., and Dobson, C. M. (1998) Folding kinetics of the SH3 domain of PI3 kinase by real-time NMR combined with optical spectroscopy. *J. Mol. Biol. 276*, 657−667.
(8) Lakshmikanth, G. S., Sridevi, K., Krishnamoorthy, G., and Udgaonkar, J. B. (2001) Structure is lost incrementally during the unfolding of barstar. *Nat. Struct. Biol. 8*, 799−804.
(9) Sridevi, K., Lakshmikanth, G. S., Krishnamoorthy, G., and Udgaonkar, J. B. (2004) Increasing stability reduces conformational heterogeneity in a protein folding intermediate ensemble. *J. Mol. Biol. 337*, 699−711.
(10) Jha, S. K., Dhar, D., Krishnamoorthy, G., and Udgaonkar, J. B. (2009) Continuous dissolution of structure during the unfolding of a small protein. *Proc. Natl. Acad. Sci. U.S.A. 106*, 11113−11118.
(11) Ratner, V., Sinev, M., and Haas, E. (2000) Determination of intramolecular distance distribution during protein folding on the millisecond timescale. *J. Mol. Biol. 299*, 1363−1371.
(12) Ben Ishay, E., Rahamim, G., Orevi, T., Hazan, G., Amir, D., and Haas, E. (2012) Fast Subdomain Folding Prior to the Global Refolding Transition of *E. coli* Adenylate Kinase: A Double Kinetics Study. *J. Mol. Biol. 423*, 613−623.
(13) Ratner, V., Amir, D., Kahana, E., and Haas, E. (2005) Fast collapse but slow formation of secondary structure elements in the refolding transition of *E. coli* adenylate kinase. *J. Mol. Biol. 352*, 683−699.
(14) Lyubovitsky, J. G., Gray, H. B., and Winkler, J. R. (2002) Mapping the cytochrome C folding landscape. *J. Am. Chem. Soc. 124*, 5481−5485.
(15) Pletneva, E. V., Gray, H. B., and Winkler, J. R. (2005) Snapshots of cytochrome c folding. *Proc. Natl. Acad. Sci. U.S.A. 102*, 18397−18402.
(16) Kimura, T., Lee, J. C., Gray, H. B., and Winkler, J. R. (2007) Site-specific collapse dynamics guide the formation of the cytochrome c′ four-helix bundle. *Proc. Natl. Acad. Sci. U.S.A. 104*, 117−122.
(17) Hutnik, C. M., and Szabo, A. G. (1989) A time-resolved fluorescence study of azurin and metalloazurin derivatives. *Biochemistry 28*, 3935−3939.
(18) Chen, L. X., Longworth, J. W., and Fleming, G. R. (1987) Picosecond time-resolved fluorescence of ribonuclease T1. A pH and substrate analogue binding study. *Biophys. J. 51*, 865−873.
(19) Beechem, J. M., and Brand, L. (1985) Time-resolved fluorescence of proteins. *Annu. Rev. Biochem. 54*, 43−71.
(20) Ababou, A., and Bombarda, E. (2001) On the involvement of electron transfer reactions in the fluorescence decay kinetics heterogeneity of proteins. *Protein Sci. 10*, 2102−2113.
(21) Engelborghs, Y. (2003) Correlating Protein Structure and Protein Fluorescence. *J. Fluoresc. 13*, 9−16.
(22) Bajzer, Z., and Prendergast, F. G. (1993) A model for multiexponential tryptophan fluorescence intensity decay in proteins. *Biophys. J. 65*, 2313−2323.

(23) Chen, Y., and Barkley, M. D. (1998) Toward understanding tryptophan fluorescence in proteins. *Biochemistry 37*, 9976−9982.
(24) Kim, S. J., Chowdhury, F. N., Stryjewski, W., Younathan, E. S., Russo, P. S., and Barkley, M. D. (1993) Time-resolved fluorescence of the single tryptophan of *Bacillus stearothermophilus* phosphofructokinase. *Biophys. J. 65*, 215−226.
(25) Dahms, T. E. S., and Szabo, A. G. (1997) Conformational heterogeneity in crystalline proteins: Time-resolved fluorescence studies. *Methods Enzymol. 278*, 202−221.
(26) Adams, P. D., Chen, Y., Ma, K., Zagorski, M. G., Sönnichsen, F. D., McLaughlin, M. L., and Barkley, M. D. (2002) Intramolecular quenching of tryptophan fluorescence by the peptide bond in cyclic hexapeptides. *J. Am. Chem. Soc. 124*, 9278−9286.
(27) Muñoz, V. (2007) Conformational dynamics and ensembles in protein folding. *Annu. Rev. Biophys. Biomol. Struct. 36*, 395−412.
(28) Tollinger, M., Skrynnikov, N. R., Mulder, F. A., Forman-Kay, J. D., and Kay, L. E. (2001) Slow dynamics in folded and unfolded states of an SH3 domain. *J. Am. Chem. Soc. 123*, 11341−11352.
(29) Hoffmann, A., Nettels, D., Clark, J., Borgia, A., Radford, S. E., Clarke, J., and Schuler, B. (2011) Quantifying heterogeneity and conformational dynamics from single molecule FRET of diffusing molecules: Recurrence analysis of single particles (RASP). *Phys. Chem. Chem. Phys. 13*, 1857−1871.
(30) Chattopadhyay, K., Elson, E. L., and Frieden, C. (2005) The kinetics of conformational fluctuations in an unfolded protein measured by fluorescence methods. *Proc. Natl. Acad. Sci. U.S.A. 102*, 2385−2389.
(31) Alcala, J. R., Gratton, E., and Prendergast, F. G. (1987) Interpretation of fluorescence decays in proteins using continuous lifetime distributions. *Biophys. J. 51*, 925−936.
(32) Lasagna, M., Gratton, E., Jameson, D. M., and Brunet, J. E. (1999) Apohorseradish peroxidase unfolding and refolding: Intrinsic tryptophan fluorescence studies. *Biophys. J. 76*, 443−450.
(33) Vix, A., and Lami, H. (1995) Protein fluorescence decay: Discrete components or distribution of lifetimes? Really no way out of the dilemma? *Biophys. J. 68*, 1145−1151.
(34) Livesey, A. K., and Brochon, J. C. (1987) Analyzing the distribution of decay constants in pulse-fluorimetry using the maximum entropy method. *Biophys. J. 52*, 693−706.
(35) Swaminathan, R., and Periasamy, N. (1996) Analysis of fluorescence decay by the maximum entropy method: Influence of noise and analysis parameters on the width of the distribution of lifetimes. *Proc.—Indian Acad. Sci., Chem. Sci. 108*, 39−49.
(36) Leenders, R., Van Hoek, A., Van Iersel, M., Veeger, C., and Visser, A. J. (1993) Flavin dynamics in oxidized *Clostridium beijerinckii* flavodoxin as assessed by time-resolved polarized fluorescence. *Eur. J. Biochem. 218*, 977−984.
(37) Sarkar, S. S., Udgaonkar, J. B., and Krishnamoorthy, G. (2011) Reduced fluorescence lifetime heterogeneity of 5-fluorotryptophan in comparison to tryptophan in proteins: Implication for resonance energy transfer experiments. *J. Phys. Chem. B 115*, 7479−7486.
(38) Graña-Montes, R., de Groot, N. S., Castillo, V., Sancho, J., Velazquez-Campoy, A., and Ventura, S. (2012) Contribution of disulfide bonds to stability, folding, and amyloid fibril formation: The PI3-SH3 domain case. *Antioxid. Redox Signaling 16*, 1−15.
(39) Booker, G. W., Gout, I., Downing, A. K., Driscoll, P. C., Boyd, J., Waterfield, M. D., and Campbell, I. D. (1993) Solution structure and ligand-binding site of the SH3 domain of the p85 α subunit of phosphatidylinositol 3-kinase. *Cell 73*, 813−822.
(40) O'Connor, D. V., and Phillips, D. (1984) *Time-Correlated Single Photon Counting*, Academic Press Inc., London.
(41) Swaminathan, R., Krishnamoorthy, G., and Periasamy, N. (1994) Similarity of fluorescence lifetime distributions for single tryptophan proteins in the random coil state. *Biophys. J. 67*, 2013−2023.
(42) Royer, C. A., Mann, C. J., and Matthews, C. R. (1993) Resolution of the fluorescence equilibrium unfolding profile of trp aporepressor using single tryptophan mutants. *Protein Sci. 2*, 1844−1852.
(43) Goldenberg, D. P. (2003) Computational Simulation of the Statistical Properties of Unfolded Proteins. *J. Mol. Biol. 326*, 1615−1633.
(44) Saxena, A. M., Udgaonkar, J. B., and Krishnamoorthy, G. (2006) Characterization of intra-molecular distances and site-specific dynamics in chemically unfolded barstar: Evidence for denaturant-dependent non-random structure. *J. Mol. Biol. 359*, 174−189.
(45) Agashe, V. R., Shastry, M. C., and Udgaonkar, J. B. (1995) Initial hydrophobic collapse in the folding of barstar. *Nature 377*, 754−757.
(46) Swaminathan, R., Periasamy, N., Udgaonkar, J. B., and Krishnamoorthy, G. (1994) Molten Globule-like Conformation of Barstar: A Study by Fluorescence Dynamics. *J. Phys. Chem. 98*, 9270−9278.
(47) Swaminathan, R., Nath, U., Udgaonkar, J. B., Periasamy, N., and Krishnamoorthy, G. (1996) Motional dynamics of a buried tryptophan reveals the presence of partially structured forms during denaturation of barstar. *Biochemistry 35*, 9150−9157.
(48) Ross, J. B., Wyssbrod, H. R., Porter, R. A., Schwartz, G. P., Michaels, C. A., and Laws, W. R. (1992) Correlation of Tryptophan Fluorescence Intensity Decay Parameters with ^{1}H NMR-Determined Rotamer Conformations: [Tryptophan^2]Oxytocin. *Biochemistry 31*, 1585−1594.
(49) Moors, S. L. C., Hellings, M., De Maeyer, M., Engelborghs, Y., and Ceulemans, A. (2006) Tryptophan rotamers as evidenced by X-ray, fluorescence lifetimes, and molecular dynamics modeling. *Biophys. J. 91*, 816−823.
(50) Julien, O., Wang, G., Jonckheer, A., Engelborghs, Y., and Sykes, B. D. (2012) Tryptophan side chain conformers monitored by NMR and time-resolved fluorescence spectroscopies. *Proteins 80*, 239−245.
(51) Hellings, M., De Maeyer, M., Verheyden, S., Hao, Q., Van Damme, E. J. M., Peumans, W. J., and Engelborghs, Y. (2003) The Dead-End Elimination Method, Tryptophan Rotamers, and Fluorescence Lifetimes. *Biophys. J. 85*, 1894−1902.
(52) Hudson, B. S., Huston, J. M., and Soto-Campos, G. (1999) A Reversible "Dark State" Mechanism for Complexity of the Fluorescence of Tryptophan in Proteins. *J. Phys. Chem. A 103*, 2227−2234.
(53) Eftink, M. R. (1994) The use of fluorescence methods to monitor unfolding transitions in proteins. *Biophys. J. 66*, 482−501.
(54) Poveda, J. A., Fernández-Ballester, G., Prieto, M., and Neira, J. L. (2007) Dynamics of tryptophan in the histidine-containing phosphocarrier protein of *Streptomyces coelicolor*: Evidence of multi-state equilibrium unfolding. *Biochemistry 46*, 7252−7260.
(55) Tcherkasskaya, O., Knutson, J. R., Bowley, S. A., Frank, M. K., and Gronenborn, A. M. (2000) Nanosecond dynamics of the single tryptophan reveals multi-state equilibrium unfolding of protein GB1. *Biochemistry 39*, 11216−11226.
(56) Huang, F., Lerner, E., Sato, S., Amir, D., Haas, E., and Fersht, A. R. (2009) Time-resolved fluorescence resonance energy transfer study shows a compact denatured state of the B domain of protein A. *Biochemistry 48*, 3468−3476.
(57) Grupi, A., and Haas, E. (2011) Segmental conformational disorder and dynamics in the intrinsically disordered protein α-synuclein and its chain length dependence. *J. Mol. Biol. 405*, 1267−1283.
(58) Kuzmenkina, E. V., Heyes, C. D., and Nienhaus, G. U. (2005) Single-molecule Forster resonance energy transfer study of protein dynamics under denaturing conditions. *Proc. Natl. Acad. Sci. U.S.A. 102*, 15471−15476.
(59) Sinha, K. K., and Udgaonkar, J. B. (2005) Dependence of the size of the initially collapsed form during the refolding of barstar on denaturant concentration: Evidence for a continuous transition. *J. Mol. Biol. 353*, 704−718.
(60) Williams, C., Brochard, F., and Frisch, H. L. (1981) Polymer Collapse. *Annu. Rev. Phys. Chem. 32*, 433−451.
(61) Sherman, E., and Haran, G. (2006) Coil-globule transition in the denatured state of a small protein. *Proc. Natl. Acad. Sci. U.S.A. 103*, 11539−11543.

(62) Hofmann, H., Soranno, A., Borgia, A., Gast, K., Nettels, D., and Schuler, B. (2012) Polymer scaling laws of unfolded and intrinsically disordered proteins quantified with single-molecule spectroscopy. *Proc. Natl. Acad. Sci. U.S.A. 109*, 16155−16160.
(63) Ziv, G., and Haran, G. (2009) Protein folding, protein collapse, and Tanford's transfer model: Lessons from single-molecule FRET. *J. Am. Chem. Soc. 131*, 2942−2947.
(64) Riddle, D. S., Grantcharova, V. P., Santiago, J. V., Alm, E., Ruczinski, I., and Baker, D. (1999) Experiment and theory highlight role of native state topology in SH3 folding. *Nat. Struct. Biol. 6*, 1016−1024.
(65) Yang, Z., Lasker, K., Schneidman-Duhovny, D., Webb, B., Huang, C. C., Pettersen, E. F., Goddard, T. D., Meng, E. C., Sali, A., and Ferrin, T. E. (2012) UCSF Chimera, MODELLER, and IMP: An integrated modeling system. *J. Struct. Biol. 179*, 269−278.